Spark plasma sintering of TiNi nano-powders for biological application

To cite this article: Y Q Fu *et al* 2006 *Nanotechnology* **17** 5293

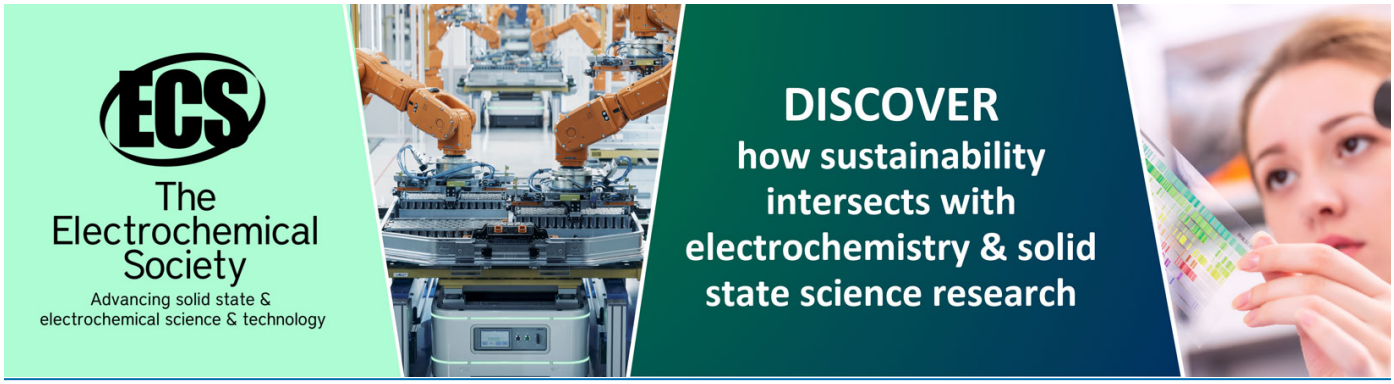

INSTITUTE OF PHYSICS PUBLISHING NANOTECHNOLOGY
Nanotechnology **17** (2006) 5293–5298 doi:10.1088/0957-4484/17/21/002

Spark plasma sintering of TiNi nano-powders for biological application

Y Q Fu[1,3], Y W Gu[1,2], C Shearwood[2], J K Luo[1], A J Flewitt[1] and W I Milne[1]

[1] Electrical Engineering Division, Department of Engineering, Cambridge University, 9 J J Thomson Avenue, Cambridge CB3 0FA, UK
[2] School of Mechanical and Aerospace Engineering, Nanyang Technological University, Nanyang Avenue, 639798, Singapore

E-mail: yf229@cam.ac.uk

Received 4 August 2006, in final form 10 September 2006
Published 6 October 2006
Online at stacks.iop.org/Nano/17/5293

Abstract
Nano-sized TiNi powder with an average size of 50 nm was consolidated using spark plasma sintering (SPS) at 800 °C for 5 min. A layer of anatase TiO_2 coating was formed on the sintered TiNi by chemical reaction with a hydrogen peroxide (H_2O_2) solution at 60 °C followed by heat treatment at 400 °C to enhance the bioactivity of the metal surface. Cell culture using osteoblast cells and a biomimetic test in simulated body fluid proved the biocompatibility of the chemically treated SPS TiNi.

1. Introduction

Titanium–nickel (TiNi) shape memory alloys (SMA) have superior properties, such as a shape memory effect, superelasticity, biocompatibility and high damping capacity, which enable them to be widely used in numerous applications. Recently there has been significant interest in the sintering of TiNi shape memory alloys using advanced powder metallurgy processes, such as self-propagating high temperature synthesis and spark plasma sintering (SPS) [1–7]. In the SPS process, a high energy, low voltage pulsed current momentarily generates extremely high and localized temperatures (up to tens of thousands of degrees) between the particles, causing the surface of the powder to vaporize and melt. SPS enables the compacted powder to be sintered to a high density at relatively low temperatures, and in a much shorter sintering time (typically a few minutes) compared to that used in conventional sintering. SPS TiNi parts are promising for biological applications, but to improve this, study of its bioactivity is necessary. Although TiNi has been proven to be biocompatible in many *in vitro* and *in vivo* studies, some concerns still remain because of its high nickel content; nickel is known to cause allergic reactions and promote carcinogenesis [8]. The osteogenesis process and osteorectin synthesis activity in TiNi alloys are problematic and the cell death rate is high on TiNi alloys compared to stainless steels and titanium alloys [9]. Moreover, it is reported that the amount of nickel released from TiNi samples prepared by powder metallurgy could be large in comparison with conventional forged/hot-rolled ones [10]. It is necessary to modify the TiNi surface to reduce the release of nickel ions and improve the biomimetic and/or bioactive properties of TiNi. Formation of a TiO_2 coating on the TiNi alloy has been considered to improve its corrosion resistance and reduce the release of metallic Ni [11]. It is also beneficial to form an anatase TiO_2 layer on TiNi alloy; thus a bone-like apatite layer could easily form on its surface in the body [12, 13]. This study will focus on the chemical treatment of the SPS sintered TiNi (with nano-powder) to form a TiO_2 layer on its surface to enhance its biocompatibility. The motives for using TiNi nano-particles are their lower melting and sintering temperatures due to their higher activation energy compared with those of conventional micrometre-sized powder. TiNi can be successfully sintered by SPS using nano-powder at 800–900 °C [7]. However, so far there have been few reports of the preparation and characterization of TiNi sintered using nano-size TiNi powder. In this study, the TiNi was prepared using SPS and the *in vitro* bioactivity of the chemically treated SPS samples was evaluated using both a cell culture method and biomimetic deposition of an apatite layer by immersing the TiNi samples into simulated body fluid (SBF).

2. Experimental details

TiNi nano-powders were prepared using the wire explosion method with TiNi wire (equiatomic 50/50 Ni/Ti atomic ratio)

[3] Author to whom any correspondence should be addressed.

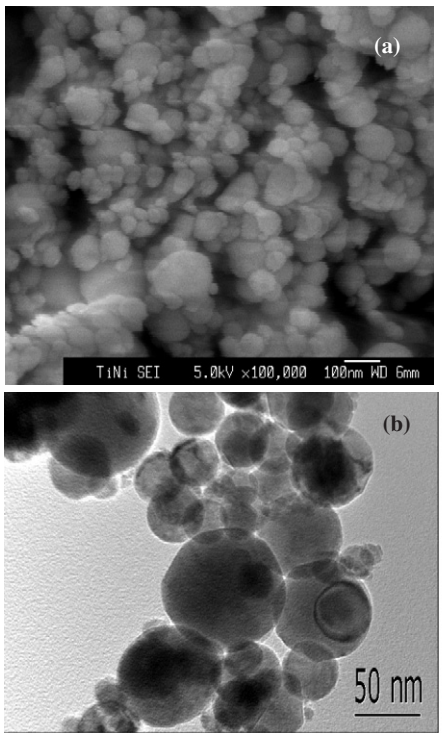

Figure 1. Morphology of nano-size TiNi powder: (a) high resolution SEM and (b) TEM.

in argon gas (99.999% purity, pressure 2 MPa) by Argonide Nanomaterials, USA [14]. The nano-TiNi powder was sintered using a DR SINTER™ type SPS 1050 (Sumitomo Coal Mining, Japan). The powder was loaded in a graphite die (13 mm in diameter) and punch unit. The vacuum level of the base chamber was less than 4.5 Pa. The pressure level was kept constant at 30 MPa throughout the sintering process. The next step is pulsed electrical discharge (860 ms on-time, 140 ms off-time, 0–1750 A, 0–5 V) followed by rapid heating. The actual densification took place during this resistance-sintering step when a high DC current was applied. The sintering temperatures were 800 °C, with a heating rate of 50 °C min^{-1}. The sintering duration was 5 min. All of the sintered specimens were mechanically ground and polished to remove any surface carbon contamination. The final sample size is about 5 mm thick with a diameter of 13 mm. The SPS TiNi samples were cleaned ultrasonically in acetone and distilled water before chemical treatment with a solution containing 8.8 M H_2O_2 and 0.1 M HCl to form a titania surface layer. The temperatures for the chemical treatment were set at 60 °C, with various times of 10, 20, 30, 40 and 60 min. They were subsequently heat treated at 400 °C for 1 h in a furnace in air.

The morphology of the nano-sized TiNi powders was characterized using a 200 kV transmission electron microscope (TEM, JEOL JEM-2000EX). The microstructure of the samples was characterized using a field emission scanning electron microscope (FE-SEM, JEOL JSM-6340F) equipped with an energy dispersive x-ray spectrometer (EDX). *In situ* crystalline structures were obtained using x-ray diffraction (XRD, Cu Kα 40 kV/40 mA) with a heating and cooling stage. Raman scattering experiments were performed using a Raman

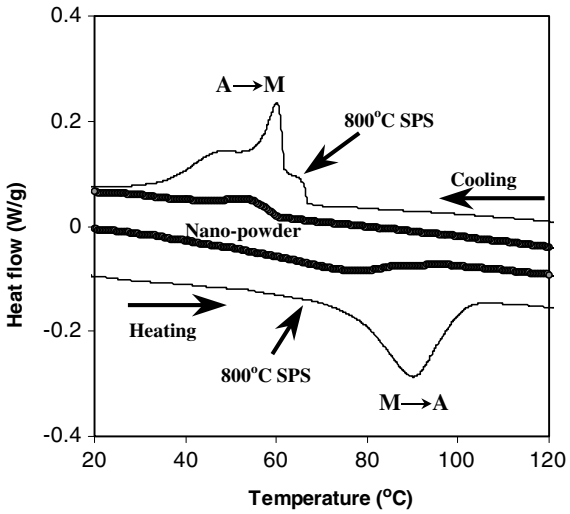

Figure 2. DSC results for TiNi nano-powders and SPS sintered TiNi alloy.

spectroscope equipped with 50 mW helium–neon laser (λ = 632.816 nm). The martensitic transformation temperatures were measured using a differential scanning calorimeter (DSC; TA Instruments, 2920 MDSC) at a heating/cooling rate of 10 K min^{-1}. Measurement was carried out under nitrogen gas flow, and calibration of temperature and heat flow was performed using an indium reference standard. The density of the sintered TiNi samples was obtained using a technique based on Archimedes' principle.

The *in vitro* cell culture work was conducted for the samples using the hFOB 1.19 cell line. This line was established by transfection of limb tissue obtained from a spontaneous miscarriage. The autoclaved SPS TiNi samples were incubated in 12-well plates using a culture medium (Dulbecco's modified Eagle's medium (DMEM) containing 10% fetal bovine serum (FBS) and 0.5% antibiotics). The cells were cultured in an atmosphere of 100% humidity, 5% CO_2, at 37 °C in 12-well culture plates (with 1 ml media contained in each well). After 2 days' incubation, the morphology of the cells attached to the samples was observed using an FE-SEM. Prior to the SEM observation, 2.5% glutaraldehyde in 0.1 M sodium cacodylate buffer was used for pre-fixing the cells, followed by post-fixation with 1% osmium tetroxide in a 0.1 M cacodylate buffer.

3. Results and discussion

3.1. SPS TiNi alloy

The high resolution SEM morphology of the TiNi nano-sized powder is shown in figure 1(a). The particles are spherical with sizes of tens of nm to 100 nm. EDX analysis indicates that the powder composition is Ti49.8Ni50.2 at.%. Figure 1(b) shows a TEM photo of the TiNi nano-powder. Selected area diffraction of TiNi particles reveals that most of these particles are single crystal in nature, being either martensite or austenite [14]. The mean grain size determined from the particle size distribution is about 50 nm.

The DSC results shown in figure 2 confirm that the TiNi nano-powder already shows phase transformation behaviour.

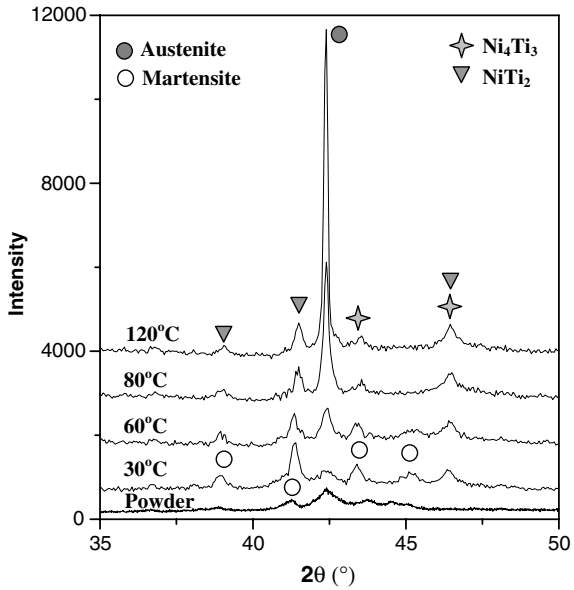

Figure 3. XRD results for TiNi powder and SPS sintered TiNi upon heating to different temperatures.

The significant broadening of the transformation peaks and hysteresis can be attributed to change in composition near the particle surface due to surface oxidation, which has the effect of removing titanium from the bulk powder [15]. The sintered TiNi specimen exhibits significant phase transformation behaviour, as shown in figure 2, compared with that of the powder. The single broad peak on the heating curve corresponds to the martensite (monoclinic) to austenite (cubic) transformation, and the two peaks on the cooling curve correspond to the transformation among austenite, R-phase and martensite.

Figure 3 shows the XRD analysis result of both the nano-size TiNi powder and the sintered specimen. Results confirm the presence of TiNi (both austenite and martensite) phases for all samples at room temperature. The broadening of different peaks for the TiNi powder indicates the tiny size of the TiNi grains, and no apparent TiO_2 phase can be detected. Compared with that of the nano-powder, the sintered TiNi specimens reveal the existence of intermediate phases, such as $NiTi_2$ and Ni_3Ti, which is common for most TiNi alloys prepared by powder metallurgy. High temperature sintering causes significant interdiffusion of atoms and leads to the formation of different types of intermetallic phases, even though only short time sintering was used in this study. The reason for this could be the reactive nature of the nano-size powder, which has a large surface/volume ratio and large activation energy. These additional phases do not exhibit a martensitic transformation or shape memory behaviour, but their formation changes the composition of the TiNi matrix and thus the transformation temperature. Figure 3 also shows the *in situ* XRD result as a function of temperature during heating. The transformation from martensite to austenite is clearly observed. At a high temperature of 120 °C, the existence of intermetallics, such as $NiTi_2$ and Ni_3Ti, can also be verified. For the sintered TiNi sample, the surfaces are shiny and metallic after polishing. The measured density of the sintered TiNi is 5.57 g cm^{-3} (that of bulk TiNi is 6.25 g cm^{-3}) and the porosity estimated using optical microscopy analysis is about 6%.

3.2. Preparation and characterization of TiO_2 layer

Figure 4 shows the surface morphology of the SPS TiNi after chemical treatment for various durations. The surface morphology of the untreated SPS TiNi is also shown in figure 4 for comparison. For the untreated SPS TiNi (figure 4(a)), the scratch marks on the surface of the sample formed during the polishing process are visible. After chemical treatment in H_2O_2/HCl solution, the surface of the TiNi appeared pale yellow in comparison with the metallic colour of the untreated ones. After chemical treatment for 20 min, the scratch marks disappear and many newly formed crystals can be observed distributed uniformly on the surface of the SPS TiNi (figure 4(b)). The number and size of the crystals increase with increasing chemical treatment time (figure 4(c)). A newly formed layer completely covers the original surface of SPS TiNi after chemical treatment for 40 min, as is evident from figure 4(d). This layer consists of many nano-sized spherical crystallites and nano-sized pores. The crystallite size ranges from 10 to 80 nm and the pore size lies in the range of 10–180 nm. After 60 min of treatment in a H_2O_2/HCl solution, a cracked thicker gel layer is obtained as shown in figure 4(e). From the EDX analysis, the surface of the SPS TiNi sample after chemical treatment for 40 min contains mainly Ti and O. From the EDX spectrum of the surface of chemically treated TiNi, there seems to be a very low Ni content, while the TiNi surface before chemical treatment shows the distinct presence of both the Ni and Ti elements. This implies that a thick layer of titanium oxide is formed on the surface of SPS TiNi after chemical treatment for 40 min.

Figure 5 shows the XRD patterns of SPS TiNi with a glancing angle of 9° after chemical treatment for 20, 40 and 60 min and subsequent heat treatment at 400 °C for 1 h. A strong peak at about 25° can be observed after chemical treatment, corresponding to the anatase phase. This implies that reaction between the Ti alloy and the H_2O_2 solution has taken place, and a titania gel layer of the form of $TiO_2{\cdot}nH_2O$, $Ti(OH)_x$ is produced [16]. This amorphous titania gel transforms to the crystalline state after heat treatment at 400 °C. It can also be observed from figure 5 that the amount of titania increases with increasing chemical treatment time, indicating an increase in the thickness of the titania layer. No nickel oxide is detected on the surface of chemically treated SPS TiNi by XRD. This is because the free energies for the formation of NiO and TiO_2 are −147 and −759 kJ mol^{-1} [17], respectively. Therefore, it is easier to form TiO_2 on the surface of the samples.

The Raman spectra of untreated and chemically treated SPS TiNi at 60 °C for 40 min are shown in figure 6. The Raman spectrum of untreated SPS TiNi is quite featureless, exhibiting hardly any peaks. After chemical treatment, anatase peaks are found on the surface of the samples, located at 142.75, 196.23, 396.87, 515.62 and 636.75 cm^{-1}, as shown in figure 6. The presence of anatase is beneficial for the bioactivity of TiNi alloy.

From the above results, an anatase layer forms on the surface of the SPS TiNi after immersion in the H_2O_2/HCl

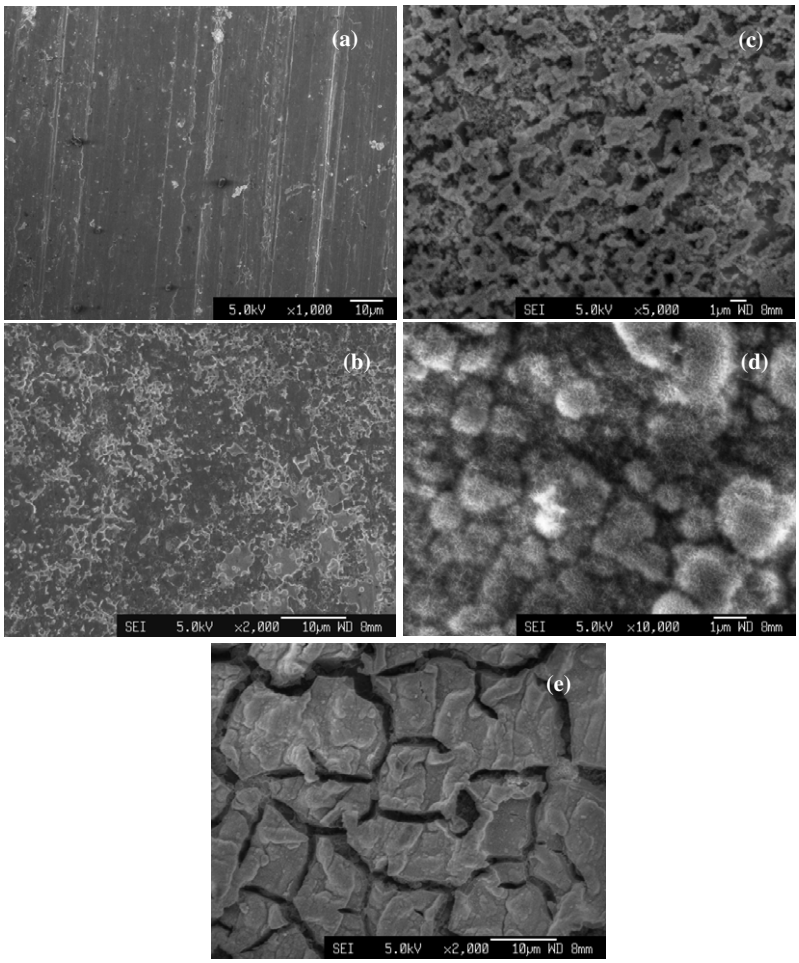

Figure 4. Surface morphology of SPS TiNi after chemical treatment for various periods of time: (a) untreated; (b) 20 min, (c) 30 min, (d) 40 min and (e) 60 min.

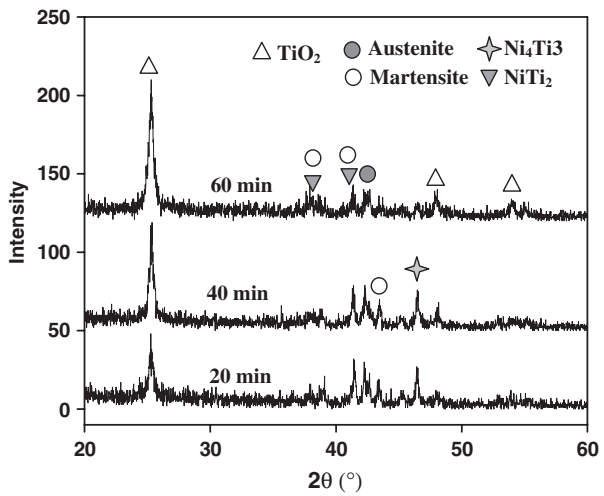

Figure 5. Thin film XRD patterns of SPS TiNi after chemical treatment for various periods of time.

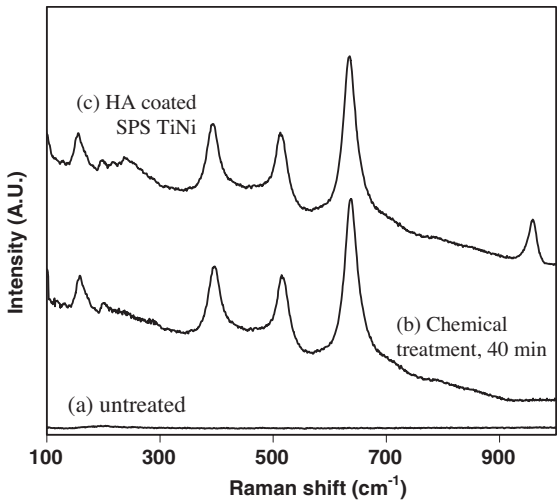

Figure 6. Raman spectra of (a) untreated, (b) chemical-treated and (c) apatite-coated SPS TiNi.

solution and post-thermal treatment. The addition of HCl to the H_2O_2 solution can speed up the reaction between the Ti and H_2O_2 and produce a clear gel morphology [18]. After chemical reaction between the Ti alloy and H_2O_2 solution, an amorphous titania gel layer of the form $TiO_2 \cdot nH_2O$ was produced based on

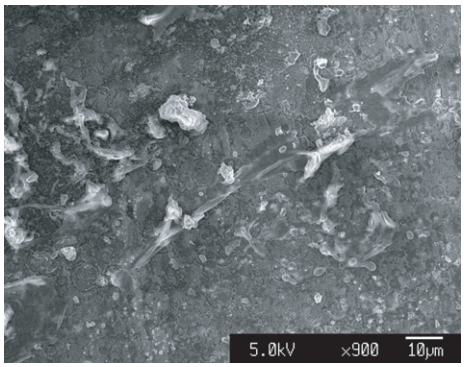

Figure 7. Typical SEM pictures showing the osteoblast cells attached to the chemically treated TiNi after 2 days of cell culture.

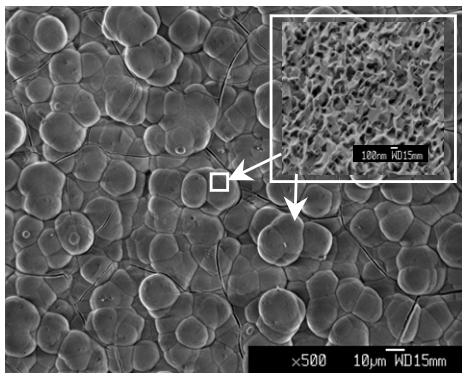

Figure 8. Surface morphology of chemically treated TiNi covered by a layer of apatite after immersion in SBF for 7 days.

reactions (1) and (2) [18]

$$\mathrm{Ti(s)} + 2\mathrm{H_2O_2} \rightarrow \mathrm{TiOOH(aq)} + \tfrac{1}{2}\mathrm{O_2(g)} + \mathrm{H_3O^+} \rightarrow \mathrm{Ti(OH)_4} \quad (1)$$

$$\mathrm{Ti(OH)_4} \rightarrow \mathrm{TiO_2(aq)} + 2\mathrm{H_2O}. \quad (2)$$

ICP analysis reveals that the Ti ion concentration in the H_2O_2/HCl solution increases during the initial period of 10 min but stabilizes afterwards. The Ni ion concentration slightly increases with chemical treatment up to 60 min, indicating a continuous release of Ni ions from the TiNi sample during chemical treatment. The release of the Ni ions from the TiNi sample to the H_2O_2 solution results in the formation of a titanium-rich phase on the sample surface. This in turns promotes the formation of the titania gel layer [15]. After heat treatment, the titania gel layer transforms into an anatase phase on the TiNi surface.

3.3. Biocompatibility

The attachment of osteoblast cells to the implant surface is a prerequisite for osteointegration of an implant. After cell culture, there are only a few cell attachments on the untreated TiNi sample after a 2-day incubation period, probably due to the presence of tiny amount of free Ni on the surface, as Ni is toxic and allergenic. Figure 7 shows the attachment of osteoblast cells on titania-coated TiNi after a 2-day incubation. Well-attached and proliferated cells can be observed, indicating fast proliferation and differentiation of the cells. Formation of an anatase TiO_2 layer could prevent the release of Ni ions from the TiNi surface. The increased attachment of osteoblast cells on the titania-coated TiNi sample can also be explained by its increased surface roughness (and thus greater surface area) compared to the non-coated sample surface, and it is well-documented that osteoblast cell proliferation is better on a rough surface [19, 20].

After immersion of the SPS TiNi sample in SBF for 2 days, some island-like particles can be observed on the surface of the chemically treated TiNi, and after 5 days the chemically treated surface is completely covered by a thick layer of uniformly spread spherical precipitates (with some small cracks observed, as shown in figure 8). High magnification observation reveals that these precipitates are composed of nano-scale, flake-like crystallites, with the typical morphology of an apatite layer. EDX results identify that these precipitates are calcium- and phosphorus-rich phases (Ca/P ratio of 1.59), which contain carbon and oxygen. The Raman spectrum is shown in figure 6. There is a strong peak at 960 cm^{-1} after immersion in SBF for 5 days. This is a characteristic peak of an apatite layer due to the symmetric stretching of the P–O mode, indicating the formation of an apatite layer on the surface of the sample [21–23]. After exposure to the SBF, the anatase layer is hydrated again to transform it into a TiO_2 hydrogel layer, which improves the formation of apatite. There is crystallographic matching between the apatite (0001) plane and the anatase (110) plane, leading to a good apatite forming ability for the anatase layer [24, 25]. Once the apatite nuclei form, they will grow spontaneously, consuming the calcium and phosphate in the SBF. A bonelike apatite layer is important for forming a strong bone-bonding interface between TiNi and living tissues. Therefore it can be concluded that with surface chemical treatment the biocompatibility of a SPS TiNi has been significantly improved.

4. Conclusions

The following conclusions can be obtained from this study:

(1) TiNi materials with apparent martensitic transformation behaviour have been successfully fabricated using nano-sized TiNi powder with an average size of 50 nm.
(2) A TiO_2 coating of anatase was found to form on the surface of SPS TiNi after chemical treatment. The amount of anatase increased with increasing chemical treatment time. Chemical treatment at 60 °C for 40 min was found to be the optimum parameter in this study.
(3) The Ti ion concentration in H_2O_2 solution was found to be stabilized after chemical treatment for 10 min, while the Ni ion concentration increased with chemical treatment time, leaving a titania-rich phase on the surface of the SPS TiNi. This resulted in the formation of a TiO_2 layer on the sample surface by a chemical reaction between the Ti and the H_2O_2 solution.
(4) Culturing of osteoblast cells on the samples showed that the chemical treatment is effective in improving the bioactivity of the samples. The promising biocompatibility of the samples is evidenced by the good attachment and proliferation of the cells.

(5) The promising biocompatibility of the samples is also evidenced by the formation of apatite layer on the surface oxidized SPS TiNi.

References

[1] Schuller E, Bram M, Buchkremer H P and Stover D 2004 *Mater. Sci. Eng.* A **378** 165
[2] Li B Y, Rong L Y, Li Y Y and Gjunter V E 2000 *Intermetallics* **8** 881
[3] Bram M, Ahmad-Khanlou A, Heckmann A, Fuchs B, Buchkremer H P and Stover D 2002 *Mater. Sci. Eng.* A **337** 254
[4] Monastyrsky G E, Odnosum V, Van Humbeeck J, Kolomytsev V I and Koval Y N 2002 *Intermetallics* **10** 95
[5] Zhao Y, Taya M, Kang Y and Kawasaki A 2005 *Acta Mater.* **53** 337
[6] Locci A M, Orru R, Gao G and Munir Z A 2003 *Intermetallics* **11** 555
[7] Shearwood C, Fu Y Q, Yu L G and Khor K A 2005 *Scr. Mater.* **52** 455
[8] Remes A and Williams D F 1992 *Biomaterials* **13** 731
[9] Shih C C, Lin S J, Chan Y l, Su Y Y, Lai S T, Wu G J, Kwok C F and Chung K H 2000 *J. Biomed. Mater., Res.* **52** 395
[10] Li Y H, Rao G B, Rong L J and Li Y Y 2004 *Mater. Sci. Eng.* R **47** 49
[11] Armitage D A and Grant D M 2003 *Mater. Sci. Eng.* A **349** 89
[12] Kokubo T, Kushitani H, Kitsugi S and Yamamuro T 1990 *J. Biomed. Mater. Res.* **24** 721
[13] Chen M F, Yang X J, Liu Y, Zhu S L, Cui Z D and Man H C 2003 *Surf. Coat. Technol.* **173** 229
[14] Fu Y Q and Shearwood C 2004 *Scr. Mater.* **50** 319
[15] Fu Y Q, Du H J, Zhang S and Huang W M 2005 *Mater. Sci. Eng.* A **403** 25
[16] Tengvall P, Elwing H and Lundstrom I 1998 *J. Colloid Interface Sci.* **130** 640
[17] Lee H G 1999 *Chemical Thermodynamics for Metals and Materials* (London: Imperial College Press) pp 275–94
[18] Gu Y W, Tay B Y, Lim C S and Yong M S 2006 *Nanotechnology* **17** 2212
[19] Wang X X, Hayakawa S, Tsuru K and Osaka A 2002 *Biomaterials* **23** 1353
[20] Tengvall P, Elwing H and Lundstrom I 1998 *J. Colloid Interface Sci.* **130** 640
[21] Wirth C, Comte V, Lagneau C, Exbrayat P, Lissac M, Jaffrezic-Renault N and Ponsonnet L 2005 *Mater. Sci. Eng.* C **25** 51
[22] Kim H M, Miyaji F, Kokubo T and Nakamura T 1996 *J. Biomed. Mater. Res.* A **32** 409
[23] Rehman I, Hench L L, Bonfield W and Smith R 1994 *Biomaterials* **15** 865
[24] Kokubo T, Kim H M and Kawashita M 2003 *Biomaterials* **24** 2161
[25] Gu Y W, Tay B Y, Lim C S and Yong M S 2005 *Biomaterials* **26** 6916